Forward Scattering from a Three Dimensional Layered Media with Rough Interfaces and Buried Object(s) by FDTD

S. H. Mirjahanmardi, P. Dehkhoda, and A. Tavakoli

Department of Electrical Engineering, Amirkabir University of Technology, Tehran, Iran
s.h.mirjahanmardi@gmail.com, pdehkhoda@aut.ac.ir, tavakoli@aut.ac.ir

Abstract − In this paper, the finite difference time domain (FDTD) method is implemented to analyze the scattered field from a three dimensional structure including two-layer rough interfaces with or without buried object(s). The effects of different parameters such as rough interface correlation length as well as its root mean square (rms) height, the moisture content of the soil, also the buried object position and size on the scattered field are studied. Simulations show that by increasing the soil moisture, the level of scattering from the structure (without the buried object) is increased. In addition, it is shown that the same amount of moisture change, but in different percentage level, shows completely different effect on the scattering level. Furthermore, it is observed that changing the correlation length in the small perturbation range does not have a significant effect on the scattering coefficients. Moreover, images from the buried objects are obtained to show the visualization of object observation with different materials in a background. The solution has been validated by the finite integration based commercial software, CST.

Index Terms − Buried object, electromagnetic scattering, finite difference time domain (FDTD), imaging, layered media, and rough surfaces.

I. INTRODUCTION

Electromagnetic scattering from rough surfaces has always been a subject of interest for scientists and researchers due to its vast range of applications. One of the most common problems related to rough surface scattering is the detection of buried objects. Cancer tissues, underground water and petroleum, and buried endangers waste are examples of buried targets to be detected. The importance and usefulness of the research on detection of buried objects is even more pronounced when it comes to have precise images in medical applications such as cancer detection. Forward scattering is the first step toward final detection.

The proposed methods in forward scattering can be categorized to analytical, semi-analytical and numerical techniques. Analytical techniques, when applicable, are the most optimal choices to solve scattering from rough surfaces without buried objects. However, for problems which include objects an extension of these techniques is possible only for canonical objects [1], [2]. Furthermore, analytical methods are limited to the region of validity [2], [3]. As an example of semi analytic approach, the extended boundary condition method has been utilized to find the scattering waves from a multilayer rough surface structure [4].

Numerical methods are neither limited to have canonical objects nor to the need of having a confined regime of validity. Hence, they are capable of solving difficult problems of scattering from stratified rough surfaces backgrounds with arbitrary shapes of embedded objects, although they are not as fast as analytical techniques. For instance, the steepest descent fast multi-pole method (SDFMM), which was introduced by Jandhyala [5], [6], is used by El-Shenawee to analyze rough layered structures with buried object(s) [7]. Several hybrid methods, such as the combination of Method of Moments (MoM) with Physical Optics (PO) approach [8] or Kirchhoff method [9] are also applied to the these types of problems.

Among the research that have been done in the area of scattering from rough surfaces media [4], [5], [10] studied the case that there is no object buried. Only a few works concentrated on the multilayer cases with object(s) [7], [8], [11], [12]. This problem will is fully studied in this paper.

One of the efficient methods to solve the scattering from rough surfaces is the finite difference time domain (FDTD) [13] solution. This method is so flexible that makes it a suitable choice to solve problems with complex geometries. In fact; when FDTD is applied to a scattering problem from buried object(s), the changes in the object(s) shape(s) and surfaces do not add significant complexity to the method. FDTD formulation also does not result in complex matrix equations (such as inverse operations) and therefore enhances the speed of calculation(s) dramatically. As an example, Kuang et al. [14] used FDTD to solve the problem of scattering from an object above a single rough layer. Also, Guo et al. has applied a parallel FDTD to the same problem [15] to make the

codes faster. These papers study the scattering from one single object located above a structure with only one rough layer.

In this paper, in order to complete our previous studies in [16], [17], a FDTD code is implemented to solve the forward scattering from a two-layer rough surfaces structure with or without a buried object(s) as shown in Fig. 1. Thereafter, the effects of different parameters such as moisture content of the background medium as well as rough surfaces parameters are studied. Up to our best of knowledge, no report which used this numerical method for composite layer includes buried objects with rough interfaces has published. In addition, the effect of moisture for different layers has not been studied using this method till now. The problem structure is shown in Fig. 1 which T1, T2 and T3 are the thickness of the upper layer, lower layer and the object location along z-direction, respectively. Notice that the bottom of the structure is truncated and an absorbing boundary is placed in order to reduce the computation space, knowing that negligible waves are reflected thereafter. T1, T2, and T3 are calculated by considering the distance between average line of the rough surfaces. The paper is organized as the following. In Section II, the model formulations as well as absorbing layer type are discussed. In Section III the convergence of the FDTD code is verified and validated by CST Microwave studio commercial software. Section IV is devoted to study the effect of different parameters of the structure and buried object(s) on scattering coefficients. The object parameters, frequency range, and surface dimensions are chosen according to [7], [14] in order to find buried metals.

II. THEORY

FDTD method has attracted many researchers attention because of its nature which can be applied to the complex structures without the need to have the problem's Green function and matrix inverse operation. In this method, Maxwell equations are discretized both in time and space domains. The explicit nature of FDTD has made it an attractive technique in terms of simplicity; however, it has its own limitation when it comes to stability conditions [18]–[20]. One of the conditions that should be satisfied in FDTD to make it stable is Courant factor constraint [21]. To avoid long text, the readers are referred to [18]–[20]. In order to apply FDTD to the models such as the one shown in Fig. 1, the whole structure should be discretized (space discretization). Because of the limitation of the computer storages, the considered space should be truncated and limited to determined edges. Due to this truncation, some portions of the waves that hit the truncated borders are reflected. These reflections produce spurious solutions and make the solution invalid; therefore, to prevent this event a specific type of layer is utilized to absorb these unwanted reflections, perfect matched layer. This absorbing layer

surrounds the truncated space, and is matched to the structure in any direction. Thus, only negligible portion of the waves will reflect back to the main space of interest. Here, we use the convolutional perfect matched layer (CPML) for our problem. This well-known type of perfect matched layer is highly effective in absorbing the evanescent waves as explained in [22].
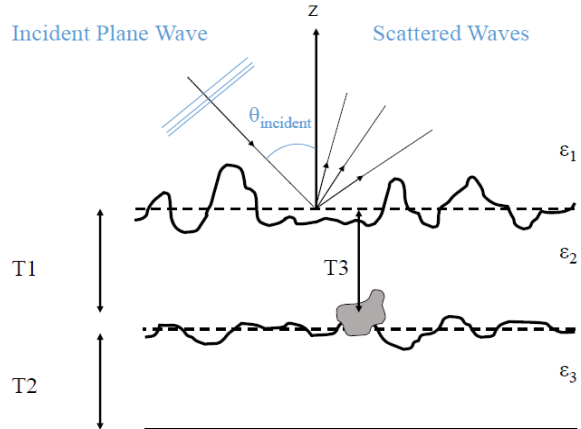
Fig. 1. A three dimensional structure with two-layered rough surfaces and a buried object, illuminated by a plane wave.

To calculate far field scattering coefficients, magnetic (A) and electric (F) potential vectors are employed and the wellknown far-field relations of [23] are used. Then, the bistatic scattering coefficient is calculated using the following equation (as stated in [24]):

$$\sigma_{pq} = \lim_{r \to \infty} \left(\frac{4\pi r^2}{S} \frac{\left| E_p^s \right|^2}{\left| E_q^i \right|^2 . cos(\theta_i)} \right), \tag{1}$$

where, subscripts p and q represent the vertical (V) and horizontal (H) polarization type of the incident and scattered fields, respectively. Also S is the total surface of the illuminated area (m^2). In addition, E^i and E^s are the incident field and the scattered field, respectively. As mentioned, the structure under the study has two rough interfaces that are created by the Gaussian function that is introduced in [25] and formulated as the following:

$$W(K_x, K_y) = \frac{h^2 l_x l_y}{4\pi} exp[-(K_x^2 l_x^2 + K_y^2 l_y^2)/4], \tag{2}$$

where, $K_x = 2x/L_x$ and $K_y = 2y/L_y$ in which L_x and L_y are the lengths of the surface along x and y directions, respectively. Also h is the root mean square (rms) height of the surface, and l_x and l_y are the correlation lengths of the rough surfaces directed in the x and y directions, respectively. Please note that in all cases presented in this paper, the ground surface along x and y directions are truncated to $L_x = L_y = 7\lambda_0$ surface. The dimension of the structure in z-direction varies case to case; therefore, the amount of that will be mentioned in each case. Please

note that as this surface is created randomly, an averaging process is necessary. In order to do that, 10 surfaces are created then averaged. In order to minimize the reflection effects of the truncations efficiently, eight CPML cells are considered at the edges of the model. The size of each cell will be stated later. An incident Gaussian plane wave with the center frequency of f_{center} and the maximum frequency of f_{max} excites the structure normally. The incident field relation is introduced in below:

$$E^i(t) = (E_V \hat{v} + E_H \hat{h}) e^{-(t-\frac{1}{c}\hat{k}.\bar{K})^2/\tau^2}, \qquad (3)$$

where E_V and E_H are the vertical and horizontal components of the electric field with their unity direction vectors ($\hat{v}$ and $\hat{h}$), respectively. c is light velocity, $\hat{k}$ is the propagation direction unity vector; R is the observing point position vector, and τ is the width of the Gaussian pulse in time domain, which can be obtained by the following relation [18]:

$$\tau = \frac{\sqrt{2.3}}{\pi f_{max}}. \qquad (4)$$

III. METHOD CONVERGENCE AND VERIFICATION

It is essential for any numerical method to be checked in order to study whether the results converge to a specific value [26] or not. In this section, the method convergence is examined. As a verification example consider the structure shown in Fig. 1 with $\epsilon_1 = 1$, $\epsilon_2 = 4.5 - j0.6$, and $\epsilon_3 = 6.5 - j0.798$. The rough surface parameters are $l_x = l_y = 0.1\lambda_0$ and h = $0.1\lambda_0$ for both interfaces. Thicknesses are $T1 = 0.4\lambda_0$ and $T2 = 1.3\lambda_0$. A perfect electric conductor (PEC) sphere with $0.2\lambda_0$ radius is placed at the center of the structure at $T3 = 0.3\lambda_0$. Where, λ_0 is the wavelength at f_{center}.

Considered incident wave is $V = \theta$ polarized with $E_\theta = 1V=m$, $f_{center} = 300$ MHz, and $f_{max} = 600$ MHz. The structure is discretized and the FDTD code is applied to calculate the total electric field (E_y) at $0.3\lambda_0$ below the object location. To obtain converged results, the cells dimension is decreased from $0.1\lambda_0$ to $0.025\lambda_0$. Then, the relative rms error is calculated in each case, which shows the amount of (E_y) convergence versus decreasing the cell size. The relative rms error at each discretization level for the E_y component is declared in Table 1. It can be realized that as the cell size is decreased, the results are converged. From here and by considering the computation time, it is decided to choose cell size of 25 mm in each direction for the simulations that are done in this study.

To evaluate the developed FDTD code, CST Microwave Studio is used as a reference [27]. Since CST does not create a Gaussian random surface, we have to consider a deterministic rough surface both in CST and our code for the validation purposes. To do this, sinusoidal interfaces with peak-to-peak value of $0.1\lambda_0$

and a number of 8 oscillations in the $7\lambda_0 \times 7\lambda_0$ truncated area are are selected. The structures parameter shown in Fig. 2 are $\epsilon_1 = 1$, $\epsilon_2 = 4.5 - j0.6$, $\epsilon_3 = 6.5 - j0.798$, $T_1 = 0.4\lambda_0$ and $T_2 = 1.3\lambda_0$. A lossy sphere with $\epsilon_2 = 2.9 - j0.0029$ and a radius of $R = 0.2\lambda_0$ is placed at $T_3 = 0.3\lambda_0$. A 1 ns delayed θ-polarized incident Gaussian plane wave illuminates the model obliquely with $\theta_i = 30°$ and $\phi_i = 0°$, where ϕ is the polar angle. Here, to avoid long text, only x-component of the magnetic field (Hx) at $0.6\lambda_0$ is shown and compared with CST in Fig. 3. As it is observed, two methods are in excellent agreement. For other observing points, the same agreement were achieved (not presented here).

Table 1: Relative error different discretization level

Cell Size ($\lambda_0 = 1m$)	Relative RMS Error (%)
0.1	--
0.06	20.65
0.05	13.81
0.04	8.36
0.03	8.01
0.025	3.65
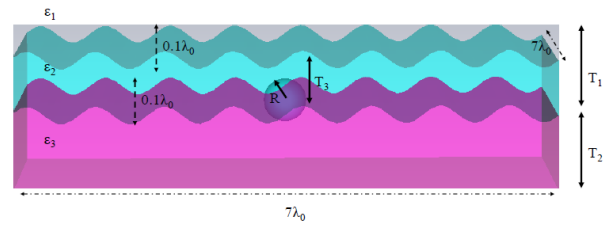
Fig. 2. Validation structure in CST. The peak to peak value for each interface is $0.1\lambda_0$. The dimensnions of the structure are $7\lambda_0 \times 7\lambda_0$ with $T_1 = 0.4 \lambda_0$ and $T_2 = 1.3\lambda_0$. A sphere with $R = 0.2\lambda_0$ is located at $T_3 = 0.3\lambda_0$. The layers materials are $\epsilon_1 = 1$, $\epsilon_2 = 4.5$-j0.6, $\epsilon_3 = 6.5$-j0.798.
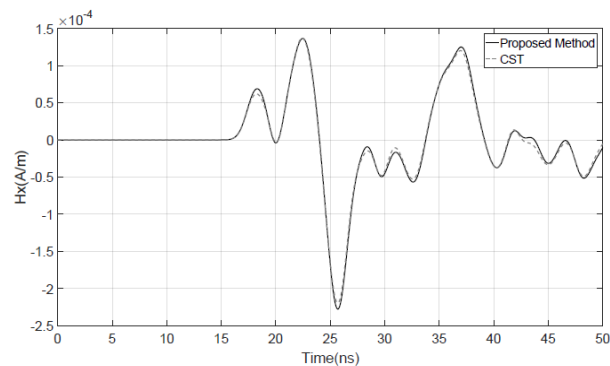
Fig. 3. The comparison between the proposed method and CST for the magnetic field in the x-direction (Hx) at $0.6\lambda_0$ below the upper rough layer. A lossy sphere with $\epsilon_r = 2.9 - j0.0029$ and the radius of $0.2\lambda_0$ is centrally placed at $T_3 = 0.3\lambda_0$.

IV. NUMERICAL RESULTS

In this section the effects of important parameters on scattering coefficients are studied. These parameters include buried object characterizes such as its depth, size, and shape as well as the background structure parameters such as correlation length, rms height of the rough interfaces, and the moisture level of the layers. For all cases, the radar cross section is normalized to the area of the truncated surface $7\lambda_0 \times 7\lambda_0$ is calculated, scattering coefficient (σ). Following subsections are devoted to the results of different case studies. In each study, the σ obtained from the model in the case that an object exists and is buried in layers are compared with the situation in which there is no object. Case study I shows the results of the structure with a buried PEC brick at different depths. In case II, the effect of correlation length of the upper rough surface is studied, while case III focuses on the rough surface rms height impact on σ. Then, the effect of moisture content of the upper layer is examined. Finally, an image of multiple objects is created.

A. Case study I

In the first attempt, consider a rectangular PEC brick with x,y, and z dimensions of $1\lambda_0 \times 1\lambda_0 \times 0.6\lambda_0$, respectively, which is buried in the model and located at the center of averaged line of a two layer structure with the following parameters: $l_x = l_y = 0.1\lambda_0$, $h = 0.1\lambda_0$, $T_1 = 0.4\lambda_0$ with $\epsilon_2 = 4.5\text{-}j0.6$ and $T_2 = 1.3\lambda_0$ with $\epsilon_3 = 6.5\text{-}j0.798$. Two vertical locations (depths) $T_3 = 0.1\lambda_0$ and $T_3 = 0.7\lambda_0$ are considered. It should be noted that the incident field normally excites the structure, and has similar properties to the incident wave introduced in Section III. The VV radar cross sections normalized to the area of the truncated surface ($7\lambda_0 \times 7\lambda_0$) for these two cases in the presence and absence of the buried object are shown in Fig. 4. In this figure, the scattered coefficient for VV case shows that when the object is placed in deeper position, the discrimination between the results of the structure with and without buried object becomes smaller. Moreover, the results from HH polarization are almost similar to the results of VV polarization with small difference in the level of scattering coefficient. Besides, if the cross polarized scattered field (VH or HV) is investigated, it can be seen that there is no rational change in them so that they are not presented here to avoid long text. More to the point, the maximum level of σ is near - 30 dB in cross polarized cases. Also, as it can be seen in Fig. 4 that the results of the three states are the same at observation around 0°. From here it is concluded that to have a better observation of the buried object a bistatic observation is supposed to be performed rather than only backscattered or specular angle.

To further examine this case; the plane wave is angled from -85° to 0°, then σ is calculated at backscattered and specular angles. Figure 5 shows these results in the presence and absence the object. In this figure, the incident angle is changed from -85° to 0° with 5° step. For the backscattered results the probe is placed in the same angle of the incident wave, while for the specular results the probe is placed at the opposite angle. Please note that increasing the object dimension increases the difference between the results with the object and without it. In addition, it is worth mentioning that it was observed that whether the object became smoother, its impact on co-polarized coefficients became less.
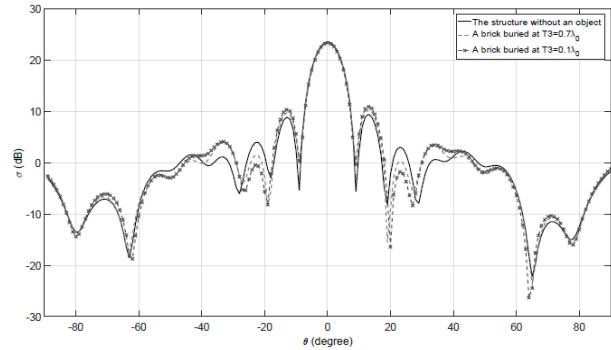
Fig. 4. VV scattering coefficient versus observation angles for three cases of the structure without buried object, buried PEC brick at $T_3 = 0.7\lambda_0$ and buried PEC brick at $T_3 = 0.1\lambda_0$. The incident wave angle is 0°, and background parameters are $l_x = l_y = 0.1\lambda_0$, $h = 0.1\lambda_0$, $T_1 = 0.4\lambda_0$, $T_2 = 1.30$, with $\epsilon_2 = 4.5\text{-}j0.6$ and $\epsilon_3 = 6.5\text{-}j0.798$.

(a)

(b)
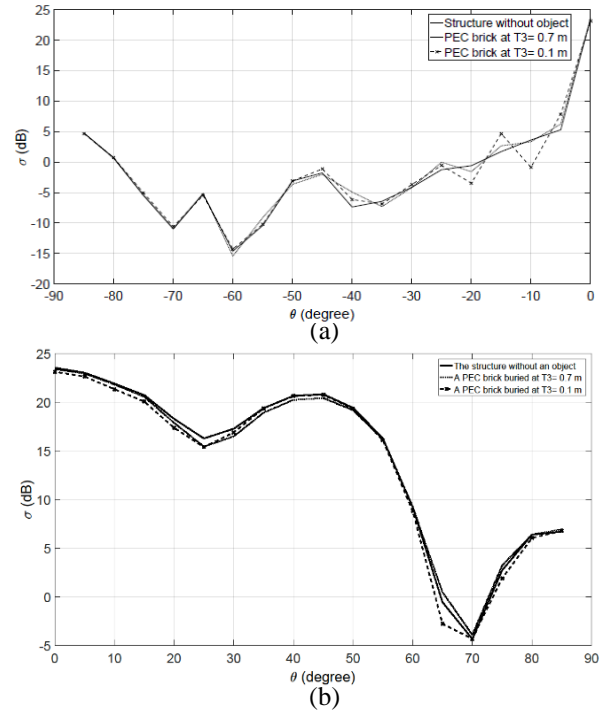
Fig. 5. (a) σ for backscattered angles and (b) specular angles in the presence and absence the PEC brick (same structure introduced in case I) for VV polarization. The step angle is 5 °.

B. Case study II

In this step, the effects of correlation lengths of the upper rough surface in the directions of x and y (l_x and l_y) on the scattering coefficient are discussed. Problem parameters are $h = 0.1\lambda_0$, $T_1 = 0.4\lambda_0$ with $\epsilon_2 = 4.5\text{-}j0.6$ and $T_2 = 1.3\lambda_0$ with $\epsilon_3 = 6.5\text{-}j0.798$. A rectangular PEC brick with $1\lambda_0 \times 1\lambda_0$ cross section and $0.6\lambda_0$ height is placed at $T_3 = 0.5\lambda_0$. In the following two studies, $l_x = l_y$ and two different values of $0.2\lambda_0$ and $0.4\lambda_0$ are considered for them. The introduced values are in the range of small perturbation [25]. In both cases, the scattering results of the structure with buried object and without it are compared. The incident wave is $V = \theta$ polarized with $E_\theta = 1V\text{=}m$, $f_{center} = 300$ MHz, and $f_{max} = 600$ MHz that illuminates the structure normally. As it can be observed in Fig. 6, the change in correlation length does not lead to significant variations in σ. The same result was obtained by Sarabandi et al. in [28].

(a)

(b)
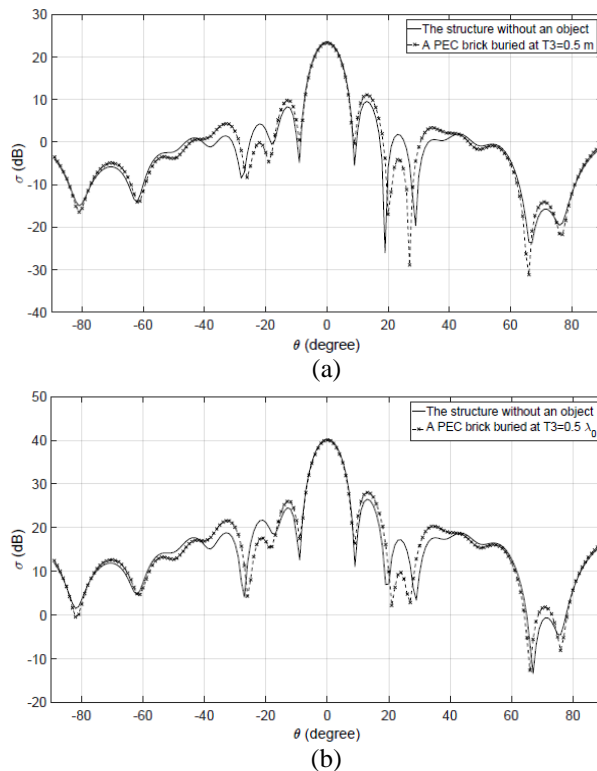
Fig. 6. Co-polorized scattering coefficient (VV) variation versus observation angle: (a) $l_x = l_y = 0.2\lambda_0$, (b) $l_x = l_y = 0.4\lambda_0$. Ground parameters are $h = 0.1\lambda_0$, $T_1 = 0.4\lambda_0$ with $\epsilon_2 = 4.5\text{-}j0.6$ and $T_2 = 1.3\lambda_0$ with $\epsilon_3 = 6.5\text{-}j0.798$. The incident wave is Gaussian with $1V\text{=}m$ amplitude and a $1\lambda_0 \times 1\lambda_0 \times 0.6\lambda_0$ PEC brick is located at $T_3 = 0.5\lambda_0$.

C. Case study III

Here we study the impact of rms height (h) of the upper rough surface on the scattering coefficient (σ). In order to investigate the effect of this parameter, rms height of the first layer is set to two values: $0.3\lambda_0$ and $3\lambda_0$. The rms height of the lower rough layer is kept constant and equal to $0.1\lambda_0$.

Layers thicknesses are $T_1 = 3.30\lambda_0$ and $T_2 = 3.0\lambda_0$, also $l_x = l_y = 0.1\lambda_0$. A $1\lambda_0 \times 1\lambda_0 \times 0.6\lambda_0$ PEC brick is buried at $T_3 = 3.50\lambda_0$. The incident wave is a Gaussian one with 1 V/m amplitude which excites the structure normally. Figure 7 shows the variation of scattering coefficient as the roughness is increasing. It can be seen that when the rms height of the upper layer is increased, the maximum level of σ is decreased. This observation means that the increase in rms height can make detecting the object more difficult. It should be noted that based on both Fig. 7 (a) and Fig. 7 (b), at some angles the difference between two curves are more than other observation angles.

D. Case study IV

In this step, the effect of content moisture of a specific soil on σ is investigated. Electromagnetically, a soil layer has four components; air, bulk soil, bound water and free water. Apparently, the complex constant of soil dielectric constant depends on the frequency. In addition, the physical temperature, the salinity, the total volumetric water content, the relative fractions of bound and free water, the bulk soil density, the shape of the soil particles, and the shape of water inclusions affects the complex dielectric constant of any soil [29].

From [29], the moisture of soil (Wv) is defined as the product of the gravimetric moisture content (Wm) and bulk density of the dry soil sample. Please note that, the gravimetric moisture content (Wm) is defined as: [(wet soil weight)-(dry soil weight)] / (dry soil weight).

We chose the upper layers soil in Fig. 1 to be similar to the soil studied in [28]. Table 2 shows its dielectric constant versus different moisture percentages.

Consider the structure with these parameters: $h = 0.1\lambda_0$, $T_1 = 0.4\lambda_0$ with the permittivity defined in Table 2, and $T_2 = 1.30$ with $\epsilon_3 = 6.5\text{-}j0.798$. Incident wave is again a Gaussian wave with 1 V/m which illuminates the model normally. A $1\lambda_0 \times 1\lambda_0 \times 0.6\lambda_0$ PEC brick is also located at $T_3 = 0.5\lambda_0$. Figure 8 shows the scattering coefficients of the structure with and without the object having the upper layer moisture level of 2.4%.

Table 2: Moisture percentage of a typical soil given in [28] and its dielectric constant

Wv (%)	Dielectric Constant
0	$3.3 - j0.35$
2.4	$3.8 - j0.50$
7.3	$4.4 - j0.63$
12	$5.1 - j0.80$
18	$8.2 - j0.40$
24	$9.8 - j1.65$
34	$15.4 - j1.65$
39	$27.1 - j2.90$
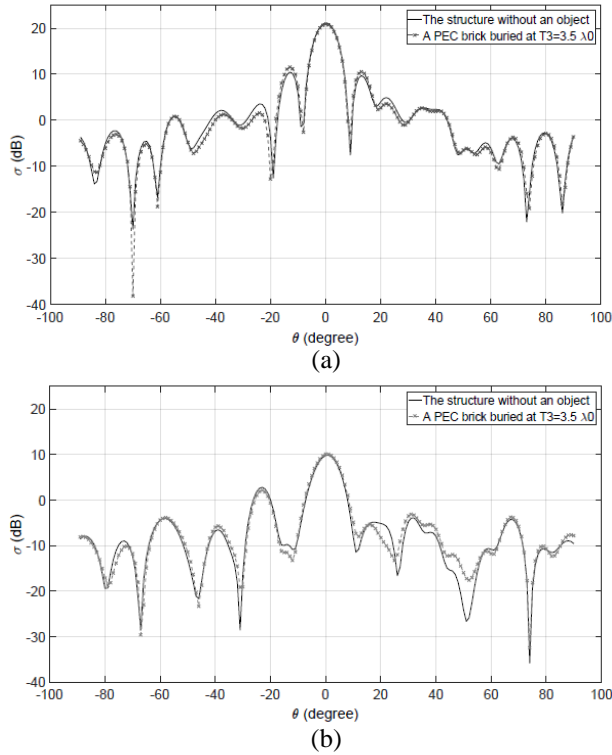
Fig. 7. Scattering coefficients for: (a) $h = 0.3\lambda_0$, and (b) $h = 3.0\lambda_0$. The structure parameters are $l_x = l_y = 0.1\lambda_0$, $h = 0.1\lambda_0$, $T_1 = 3.3\lambda_0$ with $\epsilon_2 = 4.5$-$j0.6$ and $T_2 = 3.0\lambda_0$ with $\epsilon_3 = 6.5$-$j0.798$. The incident wave is a perpendicular Gaussian with amplitude $1V=m$ and $1\lambda_0 \times 1\lambda_0 \times 0.6\lambda_0$ PEC brick is located at $T_3 = 3.5\lambda_0$.
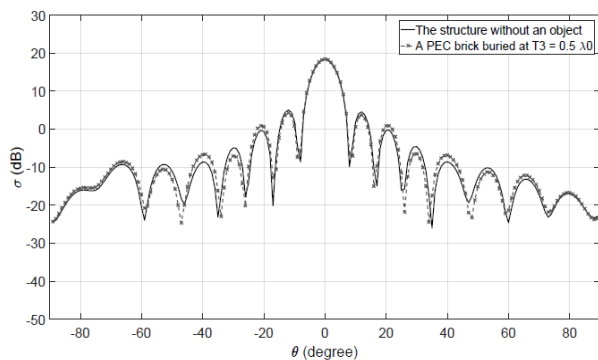
Fig. 8. VV scattering coefficient of the structure with 2.4% moisture versus observation angle for the structure without buried object, and with buried PEC brick at $T_3 = 0.5\lambda_0$ when the incident angle is normal, and background parameters are $l_x = l_y = 0.1\lambda_0$, $h = 0.1\lambda_0$, $T_1 = 0.4\lambda_0$, $T_2 = 1.3\lambda_0$, with $\epsilon_2 = 3.8$-$j0.50$ and $\epsilon_3 = 6.5$-$j0.798$.

The same process of calculating σ is done for the same structure, but with different moisture defined in Table 2. In this study, no buried object is considered and

σ of the structure for different moisture percentages are compared. It is observed that by increasing the amount of moisture, the level of scattering coefficient is increased (Fig. 9). This result is due to the effect of the moisture; it means that the higher percentage of water in soil reflects the waves more, and consequently increases the level of scattering coefficients.

The interesting point is that when the moisture percentage is changed up to 12%, the increase in σ is not as much as when the moisture increased after 18%. Also, the difference between the results in the presence of an object and it absence becomes less than 0.1 dB for 18% moisture (not shown here). In other words, as the moisture increases, two curves in Fig. 8 become more indistinguishable, and buried object detection becomes more difficult.
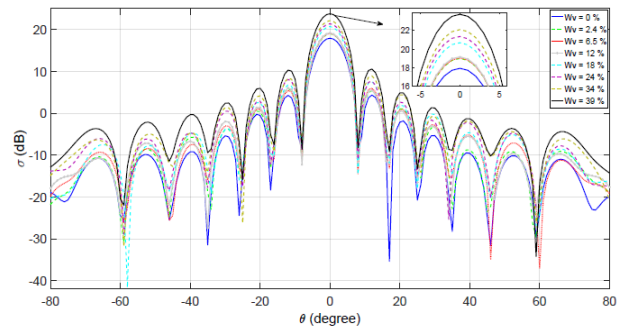
Fig. 9. VV Co-polarized scattering coefficient from a structure without object versus the level of first layer moisture level. The structure parameters are $l_x = l_y = 0.1\lambda_0$, $h = 0.1\lambda_0$, $T_1 = 0.4\lambda_0$ and $T_2 = 1.3\lambda_0$ with $\epsilon_3 = 6.5$-$j0.798$; the incident wave is $1V=m$ normal Gaussian pulse.

E. Case study V

To give the reader a visualized perspective in regards to what is done, three cubes with the same sizes ($0.5\lambda_0 \times 0.5\lambda_0 \times 0.5\lambda_0$) but different materials are buried beneath the structure in a surface which is parallel to the surface of rough interfaces in an equilateral triangular form with $2\lambda_0$ side. The depth of these three cubes is $0.5\lambda_0$. The structure is shown in Fig. 10 (a). Cube 1 is a perfect conductor with $\sigma_1 = \inf$, cube 2 is a lossy object with $\epsilon_2 = 2.9$ and $\sigma_2 = 4.3 \times 10^{-1}$, and cube 3 has $\epsilon_3 = 2.9$ and $\sigma_3 = 4.3 \times 10^{-5}$.

Figure 10 (b) is captured from the top of the first surface while looking into the medium. If the reflected waves are observed versus time; first, reflected waves from the first rough surface are received; thereafter, the reflected waves from these three cubes are observed after a while. As it is shown in Fig. 10 (b) (the image is captured when the reflections from the cubes are received) the pec cube (cube 1) has reflected the waves more than other cubes. Cube 2 which its material is different from the background's material ($\sigma = 4.3 \times 10^{-5}$)

is detectable (more wave reflections) but cube 3 which shares the same material with the background cannot be observed easily. In sum, it can be concluded that up to a specific level of similarity between the buried objects and the background, they can be detected; thereafter, it would be difficult to distinguish them from the medium. In addition, as it can be seen from the reflected waves coming from the cubes, if the objects are close to each other the coupling between them will produce ambiguities in term of the exact shape of the buried object.

(a)

(b)
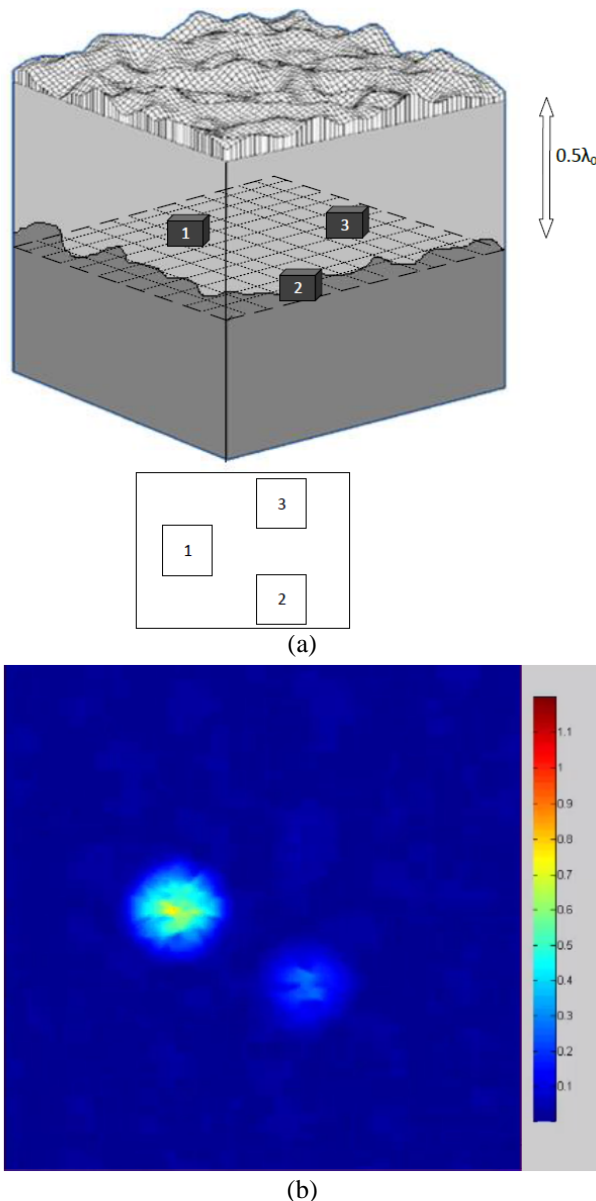
Fig. 10. (a) The structure which includes three cubes with the same size ($0.5\lambda_0$), but different materials. (b) Reflected waves captured from the top of the model when the reflection from the cubes are obtained, while looking into the depth of the system.

V. CONCLUSION

This paper was devoted to investigate the effect of some important parameters of a two layered rough surfaces medium with buried object(s) on the scattering coefficients. In the first attempt; after convergence check, the implemented code was verified by CST Microwave Studio. Studying different cases showed that when the object is placed at a deeper location, its effect on scattering coefficient becomes insignificant. Also, as the buried object size gets bigger, the scattering coefficient can be distinguished from scattering of the structure without any object. However, the effect of sharp objects such as a cube or a rectangular is more than those of smoother objects like a sphere. In another attempt, it was discussed that changing the size of correlation length in small perturbation regime had no significant effects on the results. Other observation was about the increase in rms height that could make detecting the object more difficult. Finally, it was observed that different moisture levels of soil had different effects on the scattering results. Lower moisture had lower scattering coefficient and when the moisture increased, the σ level increased. In addition, it was observed that increasing the scattering coefficient was more significant at moistures more than approximately 12%. In other words, a same amount of change but in different levels of soil moisture has completely different effects on σ.

ACKNOWLEDGMENT

REFERENCES

[1]   D. E. Lawrence and K. Sarabandi, "Electromagnetic scattering from a dielectric cylinder buried beneath a slightly rough surface," *IEEE Transactions on Antennas and Propagation*, vol. 50, no. 10, pp. 1368-1376, 2002.

[2]   M. A. Fiaz, F. Frezza, L. Pajewski, C. Ponti, and G. Schettini, "Scattering by a circular cylinder buried under a slightly rough surface: The cylindrical-wave approach," *IEEE Transactions on Antennas and Propagation*, vol. 60, no. 6, pp. 2834-2842, 2012.

[3]   J. T. Johnson and R. J. Burkholder, "Coupled canonical grid/discrete dipole approach for comput-ing scattering from objects above or below a rough interface," *IEEE Transactions on Geoscience and Remote Sensing*, vol. 39, no. 6, pp. 1214-1220, 2001.

[4]   C. H. Kuo and M. Moghaddam, "Scattering from multilayer rough surfaces based on the extended boundary condition method and truncated singular

value decomposition," *IEEE Transactions on Antennas and Propagation*, vol. 54, no. 10, pp. 2917-2929, 2006

[5] V. Jandhyala, "Fast multilevel algorithms for the efficient electromagnetic analysis of quasi-planar structures," *Department of Electrical and Computer Engineering, University of Illinois at Urbana-Champaign*, 1998.

[6] V. Jandhyala, B. Shanker, E. Michielssen, and W. C. Chew, "Fast algorithm for the analysis of scattering by dielectric rough surfaces," *JOSA A*, vol. 15, no. 7, pp. 1877-1885, 1998.

[7] M. El-Shenawee, C. Rappaport, E. L. Miller, and M. B. Silevitch, "Three-dimensional subsurface analysis of electromagnetic scattering from penetrable/PEC objects buried under rough surfaces: Use of the steepest descent fast multipole method," *IEEE Transactions on Geoscience and Remote Sensing*, vol. 39, no. 6, pp. 1174-1182, 2001.

[8] H. T. Chen and G.-Q. Zhu, "Model the electromagnetic scattering from three-dimensional PEC object buried under rough ground by mom and modified PO hybrid method," *Progress In Electromagnetics Research*, vol. 77, pp. 15-27, 2007.

[9] H. Ye and Y.-Q. Jin, "A hybrid analytic-numerical algorithm of scattering from an object above a rough surface," *IEEE Transactions on Geoscience and Remote Sensing*, vol. 45, no. 5, pp. 1174-1180, 2007.

[10] A. K. Fung, M. R. Shah, and S. Tjuatja, "Numerical simulation of scattering from three-dimensional randomly rough surfaces," *IEEE Transactions on Geoscience and remote sensing*, vol. 32, no. 5, pp. 986-994, 1994.

[11] J. He, T. Yu, N. Geng, and L. Carin, "Method of moments analysis of electromagnetic scattering from a general three-dimensional dielectric target embedded in a multilayered medium," *Radio Science*, vol. 35, no. 2, pp. 305-313, 2000.

[12] M. El-Shenawee, "Polarimetric scattering from two-layered two dimensional random rough surfaces with and without buried objects," *IEEE Transactions on Geoscience and Remote Sensing*, vol. 42, no. 1, pp. 67-76, 2004.

[13] K. Yee, "Numerical solution of initial boundary value problems involving Maxwell's equations in isotropic media," *IEEE Transactions on Antennas and Propagation*, vol. 14, no. 3, pp. 302-307, 1966.

[14] L. Kuang and Y.-Q. Jin, "Bistatic scattering from a three-dimensional object over a randomly rough surface using the FDTD algorithm," *IEEE Transactions on Antennas and Propagation*, vol. 55, no. 8, pp. 2302-2312, 2007.

[15] L.-X. Guo, J. Li, and H. Zeng, "Bistatic scattering from a three dimensional object above a two-dimensional randomly rough surface modeled with the parallel FDTD approach," *JOSA A*, vol. 26, no. 11, pp. 2383-2392, 2009.

[16] S. Mirjahanmardi, A. Tavakoli, H. Zamani, and P. Dehkhoda, "Electromagnetic scattering from a buried sphere in a two-layered rough ground," in *Antennas and Propagation & USNC/URSI National Radio Science Meeting, 2015 IEEE International Symposium on. IEEE*, pp. 506-507, 2015.

[17] S. Mirjahanmardi, A. Tavakoli, and P. Dehkhoda, "Bistatic scattering from a buried object in a two-layered media with two rough interfaces using FDTD," *ISSEEM*, 2014.

[18] A. Z. Elsherbeni and V. Demir, "The finite-difference time-domain method for electromagnetics with MATLAB simulations," *The Institution of Engineering and Technology*, 2016.

[19] U. S. Inan and R. A. Marshall, *Numerical Electromagnetics: The FDTD Method*. Cambridge University Press, 2011.

[20] A. Taflove and S. C. Hagness, *Computational Electrodynamics*. Artech House, 2005.

[21] R. Courant, K. Friedrichs, and H. Lewy, "On the partial difference equations of mathematical physics," *California Univ. Los Angeles*, Tech. Rep., 1959.

[22] J. A. Roden and S. D. Gedney, "Convolutional PML (CPML): An efficient FDTD implementation of the CFS-PML for arbitrary media," *Microwave and Optical Technology Letters*, vol. 27, no. 5, pp. 334-338, 2000.

[23] C. A. Balanis, *Antenna Theory: Analysis and Design*. John Wiley & Sons, 2016.

[24] L. Tsang, J. A. Kong, K.-H. Ding, and C. O. Ao, *Scattering of Electromagnetic Waves, Numerical Simulations*. John Wiley & Sons, vol. 25, 2004.

[25] J.-J. Wu, "Simulation of rough surfaces with FFT," *Tribology International*, vol. 33, no. 1, pp. 47-58, 2000.

[26] J. C. Rautio, "The microwave point of view on software validation," *IEEE Antennas and Propagation Magazine*, vol. 38, no. 2, pp. 68-71, 1996.

[27] CST Microwave Studio, ver. 2010, Computer Simulation Technology, Framingham, MA, 2010.

[28] K. Sarabandi and T. Chiu, "Electromagnetic scattering from slightly rough surfaces with inhomogeneous dielectric profiles," *IEEE Transactions on Antennas and Propagation*, vol. 45, no. 9, pp. 1419-1430, 1997.

[29] M. T. Hallikainen, F. T. Ulaby, M. C. Dobson, M. A. El-Rayes, and L.-K. Wu, "Microwave dielectric behavior of wet soil-part 1: Empirical models and experimental observations," *IEEE Transactions on Geoscience and Remote Sensing*, no. 1, pp. 25-34, 1985.

Seyed Hossein Mirjahanmardi received his bachelor and master degrees (with honors) from Shiraz University and Amirkabir University of Technology, respectively. He has worked on numerical electro-magnetic methods such as finite difference time domain to evaluate the scattering of rough surfaces structures. He is currently perusing his Ph.D. in Microwave Imaging at the University of Waterloo.

Parisa Dehkhoda received the B.S. degree from Tehran University, Tehran, Iran, and the M.S. and Ph.D. degrees from the Amirkabir University of Technology, Tehran, Iran, all in Electrical Engineering. She is currently an Assistant Professor in the Electrical Engineering Department, Amirkabir University of Technology. Her research interests include electromagnetic compatibility, scattering and inverse scattering, and microstrip antennas.

Ahad Tavakoli was born in Tehran, Iran, on March 8, 1959. He received the B.S. and M.S. degrees from the University of Kansas, Lawrence, KS, USA, in 1982 and 1984, respectively, and the Ph.D. degree from the University of Michigan, Ann Arbor, MI, USA, in 1991, all in Electrical Engineering. Currently, he is a Professor with the Department of Electrical Engineering, Amirkabir University of Technology, Tehran, Iran. His research interests include electromagnetic compatibility, scattering of electromagnetic waves, and microstrip antennas.